

Mechanisms controlling the SST air-sea heat flux feedback and its dependence on spatial scale

Ute Hausmann^{1,3} · Arnaud Czaja² · John Marshall¹

Received: 31 December 2015 / Accepted: 17 April 2016
© Springer-Verlag Berlin Heidelberg 2016

Abstract The turbulent air-sea heat flux feedback (α , in $\text{W m}^{-2} \text{K}^{-1}$) is a major contributor to setting the damping timescale of sea surface temperature (SST) anomalies. In this study we compare the spatial distribution and magnitude of α in the North Atlantic and the Southern Ocean, as estimated from the ERA-Interim reanalysis dataset. The comparison is rationalized in terms of an upper bound on the heat flux feedback, associated with “fast” atmospheric export of temperature and moisture anomalies away from the marine boundary layer, and a lower bound associated with “slow” export. It is found that regions of cold surface waters ($\leq 10^\circ\text{C}$) are best described as approaching the slow export limit. This conclusion is not only valid at the synoptic scale resolved by the reanalysis data, but also on basin scales. In particular, it applies to the heat flux feedback acting as circumpolar SST anomaly scales are approached in the Southern Ocean, with feedbacks of $\leq 10 \text{ W m}^{-2} \text{K}^{-1}$. In contrast, the magnitude of the heat flux feedback is close to that expected from the fast export limit over the Gulf Stream and its recirculation with values on the order of $\approx 40 \text{ W m}^{-2} \text{K}^{-1}$. Further analysis suggests that this high value reflects a compensation between a moderate thermodynamic adjustment of the boundary layer, which tends to weaken the heat flux feedback, and an enhancement of the

surface winds over warm SST anomalies, which tend to enhance the feedback.

Keywords Sea surface temperature · Air-sea interaction · Feedback · Variability · Southern Ocean · North Atlantic

1 Introduction

The rate at which sea surface temperature (SST) anomalies are damped to the atmosphere is determined to a large extent by the air-sea heat flux feedback. This quantity, hereafter denoted α_{net} (in $\text{W m}^{-2} \text{K}^{-1}$), represents the change in the net air-sea heat flux in response to a 1 K change in SST. It has been established that it varies with location, time of the year and also with the spatial scale of the SST anomaly (e.g., Frankignoul and Kestenare 2002). The heat flux feedback has been found to be a crucial parameter for a realistic representation of, for example, the ocean’s thermohaline circulation (Rahmstorf and Willebrand 1995) and the strength of decadal oscillations in the North Atlantic (NA), as shown by, for example, Czaja and Marshall (2001). More recently, its magnitude in the Southern Ocean (SO) has been identified as one of the primary sources of differences between the climate response to stratospheric ozone forcing in coupled models (Ferreira et al. 2015).

Despite its important role, observational estimates of α_{net} are sparse, especially over the SO. In a recent study, Hausmann et al. (2016) provide a benchmark calculation for the circumpolar SO, thereby complementing the previous observational estimates of α for the midlatitude ocean basins of the Northern Hemisphere and the low-latitude Southern Hemisphere (Frankignoul et al. 1998; Frankignoul and Kestenare 2002; Park et al. 2005). These studies have highlighted marked variations in α_{net} over the world’s major

✉ Ute Hausmann
uhausc@gmail.com

¹ Department of Earth Atmospheric and Planetary Sciences, Massachusetts Institute of Technology, Cambridge, MA, USA

² Department of Physics, Imperial College London, London, UK

³ Present Address: Department of Applied Ocean Physics and Engineering, Woods Hole Oceanographic Institution, Woods Hole, MA, USA

current systems. Feedbacks of typically $\approx 40 \text{ W m}^{-2} \text{ K}^{-1}$ found over the major NH boundary current systems (Gulf Stream and Kuroshio) stand in stark contrast with feedbacks of $\approx 10 \text{ W m}^{-2} \text{ K}^{-1}$ acting along the Antarctic Circumpolar Current (ACC), falling to values as low as $\approx 5 \text{ W m}^{-2} \text{ K}^{-1}$ in the region of seasonal sea ice in the summer time.

The above results are interesting but large uncertainties in estimates of α_{net} limit their usefulness. Indeed, there are not only significant uncertainties in both the turbulent and radiative components of the air-sea heat flux, but it is also difficult to isolate the component of the heat flux which responds to SST variability from that which forces it (Frankignoul et al. 1998). These uncertainties provide motivation to focus here on the mechanisms leading to the range of values cited above. We will thereby focus only on the turbulent contribution (by latent and sensible heat fluxes) to $\alpha_{net} = \alpha_{turb} + \alpha_{rad}$. As established previously for both NH and the SO (Hausmann et al. 2016), α_{turb} typically dominates the feedback. We will simply denote it α in the following (dropping the subscript).

The approach taken here is to derive bounds on the magnitude of the air-sea feedback. These provide a context for studying what sets observed spatial patterns of α . The latter can arise as a result of regional variations in the background air-sea state, but also as a result of different adjustment of the marine atmospheric boundary layer (MABL) to the underlying SST anomalies. The bounds we derive help in separating these two effects. In addition, we also partition the MABL adjustment into dynamic (i.e., involving changes in surface winds) and thermodynamic (i.e., solely involving changes in air temperature and moisture fields) components, as pioneered by Park et al. (2005) for closed ocean basins. We expand on their study and explore how the feedback and its driving mechanisms change as a function of spatial scale, moving out from the scale of atmospheric synoptic disturbances to that of ocean basins. We are particularly interested to contrast circumpolar and gyre-like oceanic regimes, and so focus on the Southern Ocean (SO) and the North Atlantic (NA) as two prototypes of these regimes, respectively.

The paper is structured as follows. In Sect. 2, upper and lower bounds on the air-sea heat flux feedback are derived using standard bulk formulae for the air-sea fluxes. These bounds are estimated using reanalysis data and compared to estimates of α in Sect. 3. Mechanisms setting the actual heat flux feedback are studied in Sect. 4. Finally, Sect. 5 provides a discussion of results and conclusions.

2 Theoretical bounds on the heat flux feedback

Turbulent air-sea heat fluxes of sensible and latent heat (Q_S and Q_L , respectively, measured positive upward, their sum being denoted Q) can be expressed via bulk formulae (e.g., Gill 1982):

$$\begin{aligned} Q_S &= \rho^a u^a c_S c_p^a (T - T^a) \\ Q_L &= \rho^a u^a c_L L (q_{sat}(T) - q^a). \end{aligned} \tag{1}$$

Here ρ^a , c_p^a , T^a and q^a are the density, specific heat capacity, temperature and specific humidity of the surface atmosphere (usually evaluated 10 m above sea-level), T and q_{sat} are temperature and specific humidity of the (saturated) ocean surface, L is the latent heat of evaporation, c_S and c_L are non dimensional transfer coefficients for sensible and latent heat flux, respectively, and $u^a \equiv |\mathbf{u}^a - \mathbf{u}|$ is the wind speed with respect to the moving ocean surface (with \mathbf{u}^a and \mathbf{u} denoting, respectively, the surface vector wind and current).

The turbulent heat flux feedback arises from the response of these turbulent fluxes to perturbations in SST. It can be expressed, in a general form, thus (e.g., Frankignoul 1985):

$$\alpha \equiv \alpha_S + \alpha_L \equiv \left. \frac{\partial \langle Q' \rangle}{\partial T'} \right|_{\bar{T}} \equiv \left. \frac{\partial \langle Q'_S + Q'_L \rangle}{\partial T'} \right|_{\bar{T}}. \tag{2}$$

In this, X' is the departure from the background seasonal state \bar{X} of a variable X , and $\langle \rangle$ denotes ensemble averaging over many realizations of the same SST anomaly. Note that the sign convention is thus that positive values of α correspond to a negative feedback on the SST anomaly.

In the absence of dynamic adjustments to SST of the atmospheric boundary layer (an assumption that is relaxed in Sect. 4), the sensible and latent components of the turbulent heat flux feedback (2) are given by

$$\alpha_S \approx \frac{\partial \langle (T - T^a)' \rangle}{\partial T'} \frac{1}{\rho^a u^a c_S c_p^a}, \tag{3}$$

and

$$\alpha_L \approx \frac{\partial \langle (q_{sat}(T) - q^a)' \rangle}{\partial T'}. \tag{4}$$

The latter expression can be further simplified using a Taylor expansion of q_{sat} :

$$q'_{sat}(T) = q_{sat}(T) - q_{sat}(\bar{T}) \approx \left. \frac{dq_{sat}}{dT} \right|_{\bar{T}} T', \tag{5}$$

and likewise,

$$q'_{sat}(T^a) = q_{sat}(T^a) - q_{sat}(\bar{T}^a) \approx \left. \frac{dq_{sat}}{dT} \right|_{\bar{T}^a} T^{a'}. \tag{6}$$

Furthermore introducing the relative humidity¹ $r_H = q^a/q_{sat}(T^a)$, the MABL specific humidity response to an SST anomaly is approximated as

¹ Strictly speaking the relative humidity is defined as the ratio of partial pressure of vapor, but we will neglect the very small difference introduced by our definition.

Table 1 Physical parameters used in the study, and their values, if assumed constant

c_p^a	Specific heat of air	1004 J K ⁻¹ kg ⁻¹
L	Latent heat of evaporation	2.5 10 ⁶ J kg ⁻¹
ρ^a	Air density	1.22 kg m ⁻³
p	Sea-level pressure	1015 hPa
c_S	Transfer coefficient for sensible heat	1.15 10 ^{-3a}
c_L	Transfer coefficient for latent heat	1.15 10 ^{-3a}
c_p	Specific heat of seawater	4000 J K ⁻¹ kg ⁻¹
ρ_0	Density of seawater	1025 kg m ⁻³

^a As recommended by Fairall et al. (2003)

$$\frac{\partial \langle q^{a'} \rangle}{\partial T'} \approx \overline{r_H} \frac{dq_{sat}}{dT} \Big|_{\overline{T^a}} \frac{\partial \langle T^{a'} \rangle}{\partial T'} + \frac{\partial \langle r_H' \rangle}{\partial T'} q_{sat}(\overline{T^a}). \quad (7)$$

In (7), the first term on the rhs represents the change in q^a arising from adjustments in air temperature at fixed relative humidity, and the second term represents the change in q^a resulting, at fixed air temperature, from adjustments in relative humidity. This enables the latent heat flux feedback (4) to be reexpressed as

$$\alpha_L \approx \overline{\rho^a u^a c_L L} \left(\frac{dq_{sat}}{dT} \Big|_{\overline{T}} - \overline{r_H} \frac{dq_{sat}}{dT} \Big|_{\overline{T^a}} \frac{\partial \langle T^{a'} \rangle}{\partial T'} - q_{sat}(\overline{T^a}) \frac{\partial \langle r_H' \rangle}{\partial T'} \right). \quad (8)$$

To understand the mechanisms setting α , let us now consider two idealized scenarios.

Limit (I): Fast export limit. In this limit we assume that the atmosphere efficiently exports any temperature and moisture anomaly developing locally in the MABL in response to an SST anomaly, so that $\partial \langle T^{a'} \rangle / \partial T' = 0$ and $\partial \langle q^{a'} \rangle / \partial T' = 0$. This can be achieved either laterally, i.e., advecting anomalies to other regions of the MABL, or vertically, by transporting anomalies upward into the free troposphere. Since the thermodynamic imbalance between air and water is maintained, the negative feedback in this limit is the largest possible and thus provides an upper bound ($\equiv \alpha_{upper}$) on α . Note that, from (7), this limit also implies that $\partial \langle r_H' \rangle / \partial T' = 0$. Using this result, and Eqs. (3) and also (8), one obtains:

$$\alpha_{upper} = \overline{\rho^a u^a} \left(\overline{c_S c_p^a} + \overline{c_L L} \frac{dq_{sat}}{dT} \Big|_{\overline{T}} \right). \quad (9)$$

Limit (II): Slow export limit. In the limit in which the atmospheric export of moisture and temperature anomaly is negligible, a thermodynamic equilibrium between air and water is achieved. In this equilibrated state there is no sensible or latent heat flux anomaly, and $\alpha \rightarrow 0$. We clearly do not expect this limit to be observed as there

is always enough turbulence and large scale motions to pull away the MABL from thermodynamic equilibrium. Observations of relative humidity over the extra-tropical oceans, however, suggest only moderate variability at low levels, on the order of 10–20 % in the monthly mean (e.g., Liu et al. 1991). Thus a more plausible limit is that in which the MABL thermally adjusts to the ocean, yet without a noticeable change in relative humidity, i.e., $\partial \langle T^{a'} \rangle / \partial T' = 1$ and $\partial \langle r_H' \rangle / \partial T' = 0$. Using these values in (3) and (8), we obtain a lower bound ($\equiv \alpha_{lower}$) on the heat flux feedback,

$$\alpha_{lower} = \overline{\rho^a u^a c_L L} \left(\frac{dq_{sat}}{dT} \Big|_{\overline{T}} - \overline{r_H} \frac{dq_{sat}}{dT} \Big|_{\overline{T^a}} \right). \quad (10)$$

Note that in this limit, there is no sensible contribution to the feedback (thermal equilibration) and that the remaining response of the latent flux arises as a result of changes in specific humidity at fixed relative humidity, i.e., $q^{a'}$ is driven solely by temperature changes.

While the expressions (3) and (4) have been derived before (e.g., Frankignoul et al. 1998), the lower bound limit (10) on the turbulent heat flux feedback has to our knowledge not been introduced previously. The upper bound limit (9) has been discussed by Frankignoul (1985) and Frankignoul et al. (1998), and also provides the basis for the zonal-average calculations by Haney (1971).

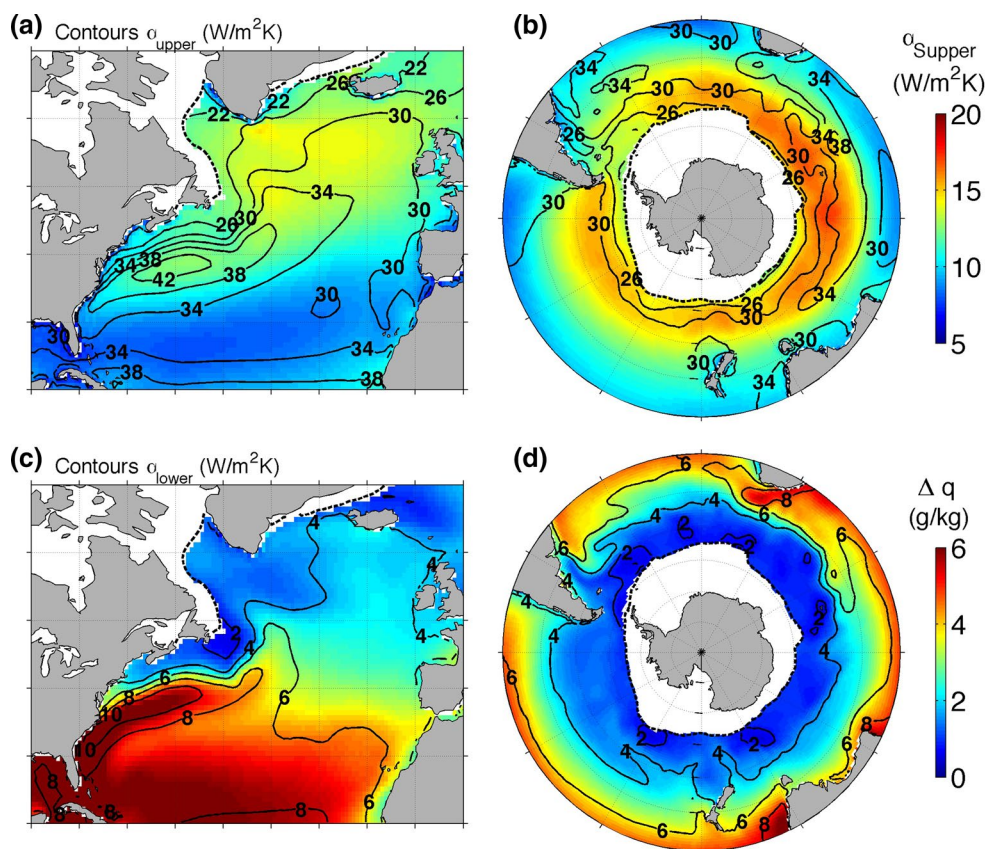
3 Application to ERA-I data in the North Atlantic and the Southern Ocean

3.1 An estimate of the lower and upper bounds

The bounds (9) and (10) are fully constrained by the background air-sea state and can thus be estimated from air-sea climatology. The ERA-Interim reanalysis dataset (Dee et al. 2011, hereafter referred to as ERA-I) is used to estimate $\overline{u^a}$, $\overline{q^a}$, $\overline{T^a}$ and \overline{T} , based on the 34-year period September 1979 to August 2013. The data is available on a 0.75° grid and results are masked within the reanalysis' seasonal sea-ice edge (15 % threshold on sea-ice concentration, denoted c hereafter). Typical values are used for other variables in (9) and (10), as listed in Table 1, and the background air-sea speed difference is approximated with the surface wind speed climatology. The bounds are estimated for each month of the year and then averaged to yield annual-mean maps.

Figure 1a, b display the estimated upper bound on the turbulent air-sea feedback, α_{upper} (black contours). Its magnitude is found to be typically 25–30 W m⁻² K⁻¹ over the ACC and the NA subpolar gyre, increasing to ≥ 35 W m⁻² K⁻¹ in NA tropics and ≈ 40 W m⁻² K⁻¹ over the warm waters on the equatorward flank of the Gulf Stream.

Fig. 1 Contours of the reference thermodynamic bounds on the turbulent (= latent + sensible) air-sea feedback, in $\text{W m}^{-2} \text{K}^{-1}$, for NA and SO: **a, b** display α_{upper} as given by (9), and **c, d** α_{lower} as given by (10). Colors in **a, b** show the sensible contribution to α_{upper} , in $\text{W m}^{-2} \text{K}^{-1}$, and in **c, d** the air-sea humidity contrast $\Delta q \equiv q_{sat}(\bar{T}) - \bar{q}^a$, in g/kg . The dashed black contour indicates the 15 % isoline of the end-winter (NA: February, SO: October) climatological sea-ice concentration.



The lower bound α_{lower} is shown in Fig. 1 in the same format (black contours), and is characterized by much weaker values, of typically only $\approx 5 \text{ W m}^{-2} \text{K}^{-1}$.

Whereas α_{lower} is set by latent heat fluxes only, α_{upper} also depends on sensible heat fluxes (Sect. 2). Figure 1a, b (color) indicate that the latter explain approximately half of α_{upper} at high latitudes. At lower latitudes, over the warm waters of the NA subtropics and tropics, the sensible contribution is of less importance. Here the latent heat flux contribution to the feedback [second term on the rhs of (9)] dominates α_{upper} as a result of its strong SST dependence.

From (9) it is clear that both background wind speed (\bar{u}^a) and SST (\bar{T}) potentially control the spatial structure of α_{upper} . The latter effect is seen in the slow increase in magnitude of α_{upper} away from the pole in the SO (Fig. 1b). The NA, which spans a broader range of latitudes and includes warmer background SSTs, features larger variations and higher peaks in the air-sea feedback strength. The oceanic flow distorts the background SST field particularly strongly over the Gulf Stream, leading to a large peak in α_{upper} over the warm tongue of the Gulf Stream, as well as to its sharp decline across the SST front marking the Gulf Stream North Wall (Fig. 1a). Another drop is observed to the south of the Gulf Stream warm tongue, here reflecting the effect of wind speed in (9) and the wind speed minimum in the region sandwiched between surface easterlies

and westerlies. Slightly enhanced values ($\alpha_{upper} \approx 35 \text{ W m}^{-2} \text{K}^{-1}$) are also seen over the Southern Indian ocean in Fig. 1b, and reflect the peak surface westerlies there (not shown).

The wind-speed induced patterns of α_{upper} are less pronounced in the maps of α_{lower} (Fig. 1c, d, contours). As suggested by (10), the thermodynamic imbalance between air and water must then be the primary player in setting the patterns of α_{lower} . The background air-sea humidity contrast $\Delta q \equiv q_{sat}(\bar{T}) - \bar{q}^a$ provides a simple measure of this effect, and Fig. 1c, d indeed indicates a good agreement between the spatial variations in Δq (colors) and α_{lower} (contours). Variations in Δq explain the small values of α_{lower} over the high-latitude SO, its equatorward increase, and also its peaks (at $\approx 6\text{--}10 \text{ W m}^{-2} \text{K}^{-1}$) over warm poleward-flowing western boundary current systems such as the Gulf Stream, the Agulhas Return current and the Brazil current. They also explain the reduced values ($\approx 2\text{--}4 \text{ W m}^{-2} \text{K}^{-1}$) over cold equatorward-flowing western boundary current systems such as the Labrador and Malvinas currents.

In summary, heat flux feedback bounds reveal differing regimes over the major SO and NA current systems. Over the ACC, α_{upper} is fairly uniform and rarely exceeds $25\text{--}30 \text{ W m}^{-2} \text{K}^{-1}$. In contrast a strong local maximum in excess of $40 \text{ W m}^{-2} \text{K}^{-1}$ occurs over the Gulf Stream

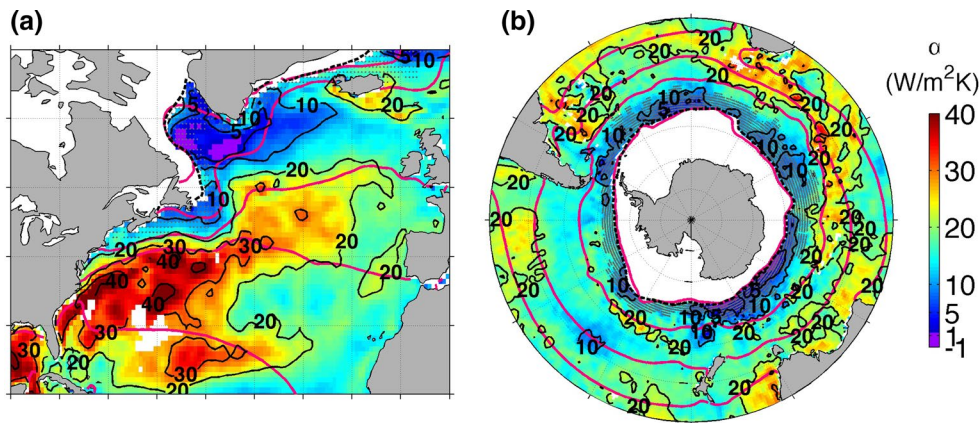


Fig. 2 The **a** NA and **b** SO turbulent feedback strength α , in $\text{W m}^{-2} \text{K}^{-1}$, estimated from ERA-I data as described in the text (colored and contoured in black). Bright red contours show climatological SST isotherms (starting at the poles: 3, 6.5, 12.5, 18.5 and 24.5 °C in the NA, and 0, 6.5, 12.5 and 18.5 °C in the SO). As in

Fig. 1, the dashed black contour indicates a sea-ice concentration c of 15% at the end of winter. Stippling indicates regions, in which the estimate of α would be unavailable if only based on Q with $c = 0\%$, rather than $c \leq 15\%$ as colored

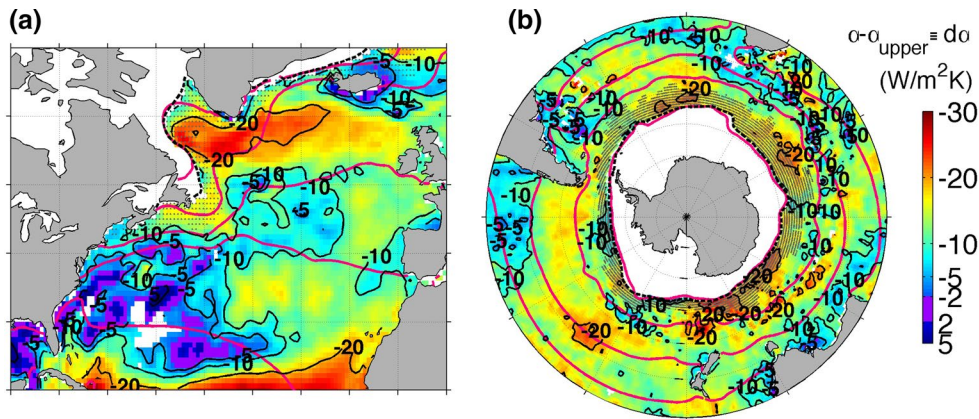


Fig. 3 **a** NA and **b** SO $d\alpha \equiv \alpha - \alpha_{upper}$, that is the departure of the actual turbulent air-sea feedback α (as mapped in Fig. 2) from its upper bound α_{upper} (as contoured in Fig. 1a, b). Otherwise as Fig. 2. Red shades indicate a feedback much lower than its upper bound

warm tongue. The lower bound α_{lower} reveals that α is not expected to drop below 8–10 $\text{W m}^{-2} \text{K}^{-1}$ over the Gulf Stream, while over the ACC it could become as low as 2–4 $\text{W m}^{-2} \text{K}^{-1}$.

3.2 Comparison with the actual turbulent heat flux feedback

As discussed in Sect. 1, several studies have produced estimates of the turbulent heat flux feedback α in the Northern Hemisphere (e.g., Frankignoul and Kestenare 2002; Park et al. 2005) and recently an estimate has become available also for the SO (Hausmann et al. 2016). Figure 2 displays an estimate of α obtained by applying the method described in this latter study (as outlined also in Appendix 1) to the ERA-I dataset, for both the NA and the SO. As in

the calculation of the bounds above, α is estimated for each month of the year, and subsequently annually averaged. The resulting annual-mean maps compare well with the previously published estimates for both the NA (Fig. 2a), and the SO (Fig. 2b—cf. to Hausmann et al. 2016, their Fig. 1a).

Comparison of Figs. 1 and 2 indicates that over the Gulf Stream the observed feedback (Fig. 2a colors) is close to its upper bound α_{upper} (Fig. 1a contours), with values of $\approx 40 \text{ W m}^{-2} \text{K}^{-1}$. This limit is also approached, but to a lesser extent, over the Agulhas region, with actual feedbacks of $\approx 25 \text{ W m}^{-2} \text{K}^{-1}$ (Fig. 2b colors) whereas $\alpha_{upper} \approx 35 \text{ W m}^{-2} \text{K}^{-1}$ (Fig. 1b contours). However, in the subtropical interiors of both hemispheres (away from the western boundaries), along the ACC, and in the subpolar gyre of the NA, α is a factor of 2 to 3 smaller than α_{upper} . The lower

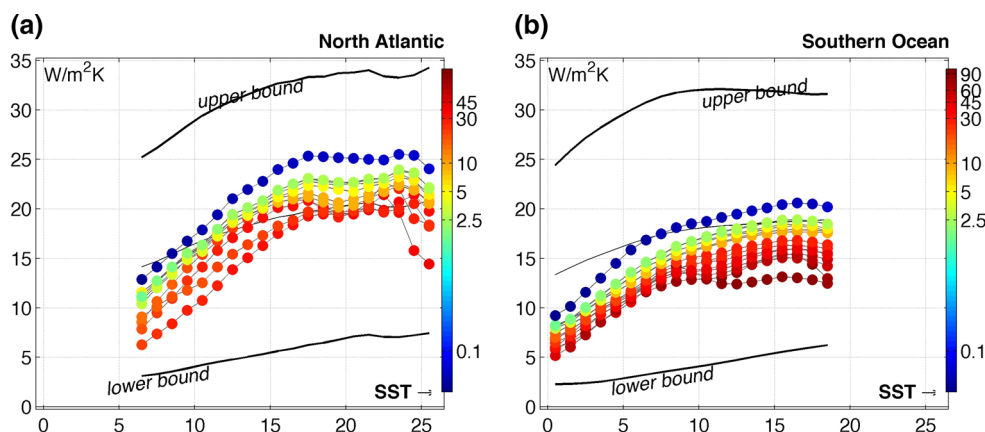


Fig. 4 **a** NA and **b** SO large-scale turbulent air-sea feedback α (y-axes, in $\text{W m}^{-2} \text{K}^{-1}$) as function of background SST (x-axes, in $^{\circ}\text{C}$) and spatial scale. Spatial scale is color-coded (as multiples of the area of a 1° longitude by 10° latitude box at 40°N/S , defining the area unit SU), increasing from the 100 km scale (blue, $\approx 1^{\circ}$ by -1° , or 0.1 SU) to basin scales (red, 30° – 90° longitude by 10° latitude, or 30–90 SU). The isotherm-average of the raw feedback calculation without

bound α_{lower} (Fig. 1c, d contours) is approached over the subpolar gyre of the NA and close to the sea-ice margin of the SO.

Figure 3 provides maps of $d\alpha \equiv \alpha - \alpha_{upper}$, in which these different regimes clearly stand out. Overall the observed heat flux feedback α lies within and spans the range between the lower and upper bounds introduced in Sect. 2. Indeed, where the bounds themselves are both lowest, such as along the poleward edge of the ACC and in the NA subpolar gyre, the actual feedback is closer to the “slow export limit”, described by the lower bound (large negative $d\alpha$, red shades in Fig. 3). In contrast, where the bounds are largest, such as over poleward-flowing western boundary current systems, exemplified here most markedly by the Gulf Stream system, the actual feedback is closer to the “fast export regime” described by the upper bound (near-zero $d\alpha$, blue shades in Fig. 3). The low-latitude NA ($\leq 25^{\circ}\text{N}$) forms an exception in this respect, as here the bounds themselves are large (due to their SST dependence), yet, as shown by the red shades in Fig. 3, the actual feedback is relatively small and drops away from the upper closer to the lower bound regime.

These previous results apply to the heat flux feedback acting at spatial scales on the order of several 100 kilometers, as resolved by the ERA-I data. As SST anomalies of larger spatial scale are considered, the “slow export” limit is expected to become more relevant as lateral advection of atmospheric temperature and moisture anomalies weakens. Adjustment to SST of the large-scale atmospheric circulation (see e.g. Ferreira et al. 2001) are furthermore anticipated to contribute to lowering the heat flux feedback towards its lower bound on larger scales. To explore this,

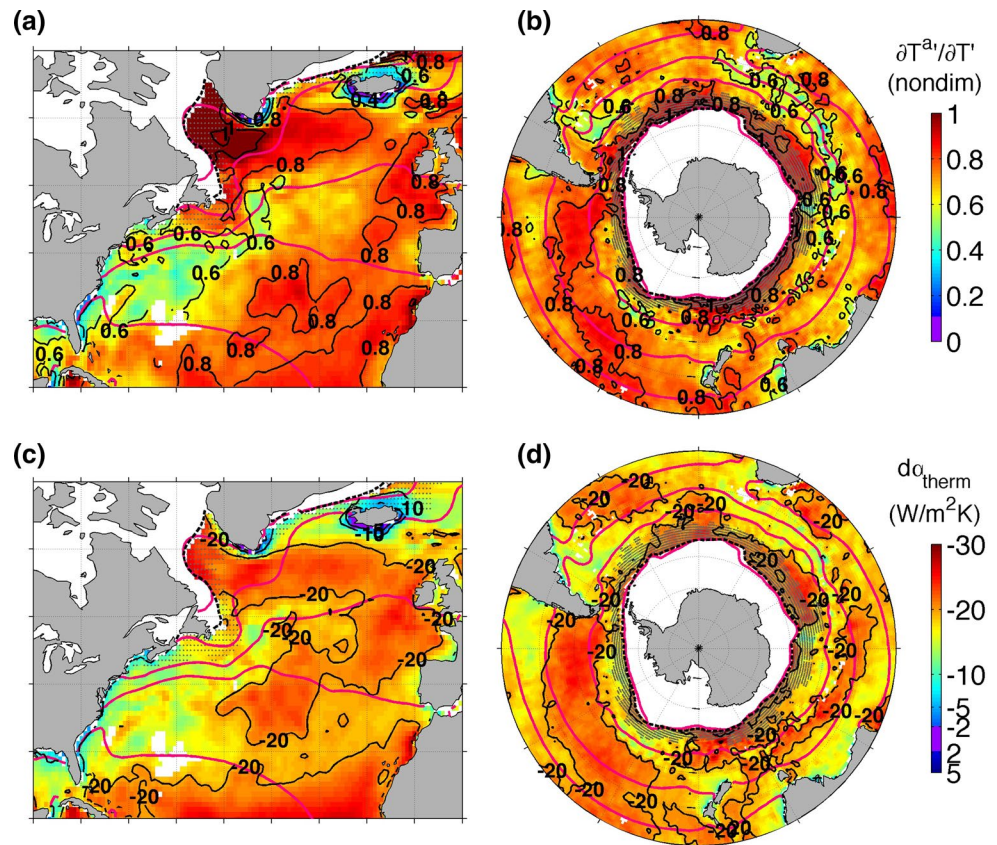
any box-averaging of ERA-I data is also indicated (in blue) and corresponds to a scale of ≈ 0.1 SU. At each larger scale, but at the largest available for the given region, two realizations of the estimate are displayed, the second of which uses coarse boxes shifted to the east by half of their zonal width. Thick black lines plot the scale-independent α_{upper} and α_{lower} , the thin line indicating $(\alpha_{lower} + \alpha_{upper})/2$

the heat flux feedback is estimated from SST and turbulent heat flux anomalies averaged over grid boxes of increasing size. The meridional extent is kept fixed at 5° latitude while the zonal extent is varied from 5° to 10° longitude. Then, at a meridional extent of 10° latitude, the zonal extent is further increased from 10° , 30° to 45° longitude, and in the SO furthermore up to 60° and 90° longitude.² The result is displayed in Fig. 4. Each marker color corresponds to a different spatial scale (box size), as indicated by the color-bar (in an area unit SU, where 1 SU is defined by the area of a 10° -latitude by 1° -longitude box at 40° latitude). The horizontal axis uses SST as a measure of location, i.e., the box-averaging is centered on the climatological mean SST contours, and a marker in the Figure displays the average over all boxes of a given size along a given isotherm.

Figure 4 shows that, for any given surface isotherm, α decreases as the spatial scale is increased (from blue to red). Conversely, the feedback overall increases with SST at a given scale. For comparison, the black curves in Fig. 4 indicate the average values of α_{upper} and α_{lower} along each climatological mean SST contour. These show that α is constrained by its bounds at all scales and overall lies in the middle of the range (as indicated by the $(\alpha_{lower} + \alpha_{upper})/2$ contour). It is seen that, in the NA (Fig. 4a), α is closer to α_{lower} than α_{upper} over cold SSTs at all spatial scales, while the reverse is true over the warm SSTs of the subtropics (only beyond 25°C feedbacks drop again). A similar trend is found over the SO, but here feedbacks remain

² As further discussed by Hausmann et al. (2016), the confidence in the estimate of α is low at larger circumpolar scales and we thus focus on basin scales and smaller here ($\leq 90^{\circ}$ longitude).

Fig. 5 **a, b** Thermal adjustment of the surface atmosphere to perturbations in SST $\partial\langle T^{a'}\rangle/\partial T'$, and **c, d** the resulting contribution the feedback, estimated as (15) (Isotherms, ice-edge and stippling as in Fig. 2)



overall closer to α_{lower} than α_{upper} also in the 15–20 °C isotherm range. This likely reflects that these SO isotherms sample both basin interiors and western boundary current regions, whereas in the NA primarily the latter. The drop of α towards α_{lower} over cold SSTs is particularly striking in the coldest SO isotherms surrounding Antarctica (red circles on Fig. 4b in the range 1–6 °C) where $\alpha \approx 5$ –10 $\text{W m}^{-2} \text{K}^{-1}$. Note that on the poleward edge of this range sea ice prevails seasonally. Repeating the estimate with Q_S and Q_L included only over sea-ice free grid points ($c = 0\%$, rather than $c \leq 15\%$ as shown) yields feedbacks that flatten off at a scale-dependent 8–13 $\text{W m}^{-2} \text{K}^{-1}$ over these coldest isotherms (not shown). This difference may point to residual sea-ice contamination in the ERA-I surface heat fluxes where $0 < c \leq 15\%$, but also likely reflect the more equatorward location of the $c > 0\%$ region (as discussed by Hausmann et al. 2016, in more detail).

4 Mechanisms

4.1 Thermal adjustment

The above results suggest that the fast export limit (corresponding to $\partial\langle T^{a'}\rangle/\partial T' = 0$, Sect. 2) is approached over the Gulf Stream on the spatial scale resolved by the

ERA-I dataset, while the slow export limit (characterized by $\partial\langle T^{a'}\rangle/\partial T' = 1$) is approached in the NA subpolar gyre and adjacent to the Antarctic winter-time sea-ice edge on these spatial scales (several 100–1000 kms), as well as along the ACC over basin-wide SST anomaly scales. This interpretation implies that there is little thermodynamic adjustment of the MABL to SST anomalies over the Gulf Stream region, yet a significant adjustment over subpolar regions of both hemispheres, and over basin-scale SO SST anomalies.

To further support this interpretation, in the following $\partial\langle T^{a'}\rangle/\partial T'$ is estimated explicitly from the data over the regions and scales considered. To do so the method that is used above to estimate α , which provides an estimate of $\partial\langle X'\rangle/\partial T'$ with $X = Q$, is instead applied to $X = T^a$. The resulting annually-averaged maps of the temperature sensitivity $\partial\langle T^{a'}\rangle/\partial T'$ are displayed in Fig. 5a, b. The Figure shows that, in agreement with the above interpretation, the temperature sensitivity is close to unity in the NA subpolar gyre and near the margin of the Antarctic winter-time sea-ice edge. The Gulf Stream in turn is seen to be the region with lowest $\partial\langle T^{a'}\rangle/\partial T'$, the value found there being in between that of the two limits ($\partial\langle T^{a'}\rangle/\partial T' \approx 0.5$). Likewise, the signature of other western boundary currents is hinted at in the SO in Fig. 5b, with local minima in the temperature sensitivity found over the Brazil-Malvinas

confluence region, and the Agulhas and its return current ($\partial\langle T^{a'}\rangle/\partial T' \approx 0.6$). Calculation of the temperature sensitivity on increasingly larger spatial scales, using the same method as described in Sect. 3b for the scale-dependence estimate of α indicates that $\partial\langle T^{a'}\rangle/\partial T'$ indeed increases on moving towards larger scales, and exceeds 0.9 in the NA/SO poleward of 50°N/S on synoptic scales and larger (not shown).

These results support the interpretation that high latitudes in the NA and the SO are close to the slow export limit. This likely reflects the fact that the atmosphere converges, in the annual mean, heat and moisture toward these regions (e.g. Trenberth et al. 2001), thereby limiting how efficiently temperature or moisture anomalies can be removed from them. Over the Gulf Stream, the $\partial\langle T^{a'}\rangle/\partial T'$ in Fig. 5a are weaker than elsewhere, consistent with this region being one of large atmospheric heat transport divergence in the mean (e.g. Trenberth et al. 2001). However, at $\partial\langle T^{a'}\rangle/\partial T' \approx 0.5$, they still imply a significant thermal adjustment of the MABL, yet the value of α is nonetheless close to that expected from the fast export limit in this region.

To understand how this can be, and quantify the impact of thermal adjustment on α , the contribution of the $\partial\langle T^{a'}\rangle/\partial T'$ term to the departure $d\alpha$ of the turbulent heat flux feedback ($\alpha = \alpha_{upper} + d\alpha$) from its upper bound α_{upper} is displayed in Figs. 5c, d (it is given by the sum of the 2nd terms on the rhs of Eqs. (3) and (8), and the estimation method is detailed in Appendix 2). It is seen to be more negative than the actual $d\alpha$ (mapped Fig. 3), over the SO, in the NA subtropics, and, in particular, over the GS region. Thus, in these regions, the presence of MABL thermal adjustment alone would yield feedbacks that are weaker in magnitude than those observed.

4.2 Other processes

To find the missing processes at work, $d\alpha$ is further decomposed into a thermodynamic adjustment component (this includes the contribution to changes in latent and sensible heat fluxes by atmospheric thermal, and moisture adjustments to SST anomalies, in the absence of changes in wind speed) and a dynamic adjustment component (solely involving changes in wind speed), thus:

$$d\alpha = d\alpha_{thdyn} + d\alpha_{dyn} + d\alpha_{res}. \quad (11)$$

The definition of the thermodynamic and dynamic terms in this equation, and how they are estimated from data, is given in Appendix 2. Note that the extra term in (11), $d\alpha_{res}$, is a residual including all terms neglected in this derivation (changes in drag coefficient, cross terms involving correlations between changes in air temperature or relative

humidity and windspeed, and the *small* higher order terms in the Taylor expansions in Sect. 2).

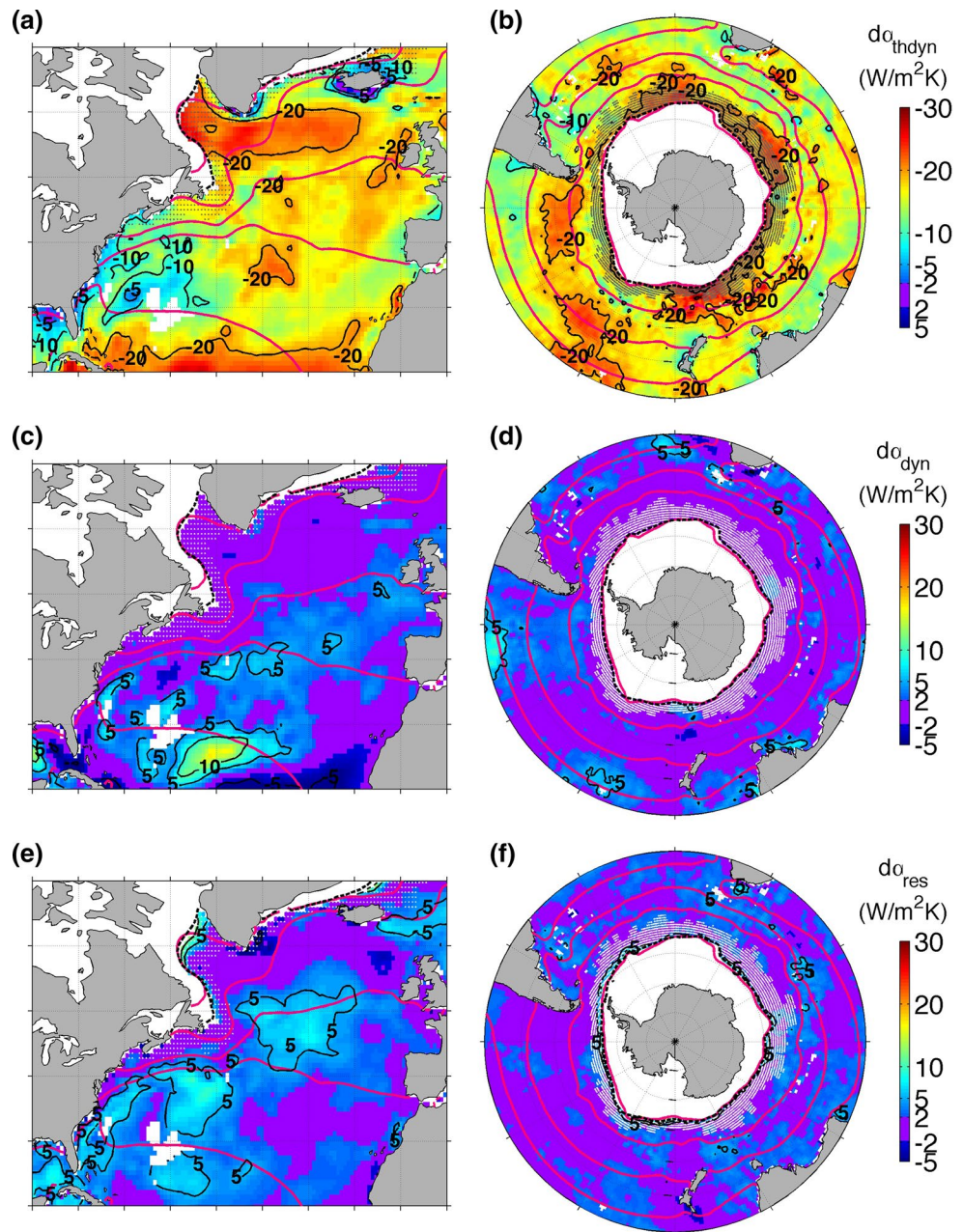
Figure 6 illustrates the partitioning of α in the framework of (11) for both the NA (left column) and the SO (right column). As expected from Sect. 4a, $d\alpha_{thdyn}$ (top row) displays large negative values at high latitudes in both domains and also approaching the tropics, whereas weak negative values prevail over the Gulf Stream.

Relative humidity adjustment This reduction of the feedback by thermodynamic adjustment ($d\alpha_{thdyn}$, Fig. 6a, b) is not as pronounced as suggested by the thermal adjustment contribution alone (Fig. 5c, d): it is less negative by +3–5 $\text{W m}^{-2} \text{K}^{-1}$ across the ACC, and the SO and NA subtropics, and by almost +10 $\text{W m}^{-2} \text{K}^{-1}$ over the Gulf Stream recirculation.

This difference must reflect a MABL that is less equilibrated in terms of moisture than suggested by the thermal adjustment alone (via $\partial\langle r'_H\rangle/\partial T' < 0$, see Eq. 7 and also Appendix 2), thereby pushing the feedback up closer towards the fast export regime despite the substantial thermal adjustment $\partial\langle T^{a'}\rangle/\partial T' \geq 0.5$ present over these regions. This is confirmed by an examination of $\partial\langle r'_H\rangle/\partial T'$, which reveal to be indeed weakly negative over these regions ($\approx -1 \text{ %/K}$), and to peak at a minimum of $\approx -2 \text{ %/K}$ over the warm flank of the Gulf Stream (not shown).

Dynamical adjustments Although weak, the $d\alpha_{thdyn}$ (Fig. 6a) over the Gulf Stream region of $\approx -10 \text{ W m}^{-2} \text{K}^{-1}$ are still larger in magnitude than the actual difference $d\alpha$ between α and α_{upper} in this region (mapped in Fig. 3a). There must thus be a mechanism compensating the thermodynamic adjustment of the boundary layer to SST anomalies in the western NA subtropical gyre. Inspection of Fig. 6c ($d\alpha_{dyn}$) and Fig. 6e ($d\alpha_{res}$) over the NA suggests that enhanced (reduced) wind speeds over warm (cold) SST anomalies account for about half ($d\alpha_{dyn} \approx +5 \text{ W m}^{-2} \text{K}^{-1}$) of the required compensation, the remaining half arising from the residual. The positive contribution $d\alpha_{dyn}$ to the south of the Gulf Stream reflects positive wind sensitivities $\partial\langle u^{a'}\rangle/\partial T'$ on the order of $0.2 \text{ m s}^{-1} \text{K}^{-1}$ (not shown). This is consistent in the sign with the enhancement of wind stress observed over time-averaged mesoscale SST features in satellite data (e.g. Chelton et al. 2004, at about half its magnitude—see O'Neill et al. 2012). Note that such a compensation between thermodynamic and dynamic effects, respectively reducing and enhancing the feedback with respect to α_{upper} , is also operative, if to a lesser degree, over the SO subtropics and its boundary currents, such as the Agulhas and its return current. In these regions the small $d\alpha_{dyn}$ and $d\alpha_{res}$ (Fig. 6d, f) enhance $d\alpha$ from the $d\alpha_{thdyn} \approx -15 \text{ W m}^{-2} \text{K}^{-1}$ (Fig. 6b) to their actual value of less than $-10 \text{ W m}^{-2} \text{K}^{-1}$ (Fig. 3b).

Fig. 6 Contributions to $d\alpha$, the departure of the air-sea feedback α from α_{upper} , as mapped in Fig. 3, reflecting: **a, b** atmospheric thermodynamic adjustments $d\alpha_{thdyn}$, estimated as (13), **c, d** atmospheric dynamic coupling $d\alpha_{dyn}$, estimated as (17), and **e, f** residual processes. Note the change of sign in the color-scale in (a, b) with respect to (c–f). (Isotherms, ice-edge and stippling as in Fig. 2)



An interesting contrast to higher latitudes, where $d\alpha_{thdyn}$ and $d\alpha_{dyn}$ consistently oppose each other (see Fig. 6a, b vs. c, d), is seen in the NA subtropics at $\approx 20^\circ\text{N}$, which features negative $d\alpha_{dyn} \approx -5 \text{ W m}^{-2} \text{ K}^{-1}$ (Fig. 6c) and thereby a cooperation of dynamical and thermodynamical processes weakening the feedback below its upper bound. Here (and also further towards the tropics of the NA, not shown) dynamical coupling provides a weak positive feedback on SST, revealing the action of a positive wind-evaporation-SST (WES) feedback (e.g. Czaja et al. 2002, and references therein). Consistent with the result of the latter

study this is not strong enough to induce a net positive air-sea feedback in this region (as seen in Fig. 2a, a negative net turbulent feedback operates here at a rate $\alpha \approx 15 \text{ W m}^{-2} \text{ K}^{-1}$). The results presented here moreover show that in the low-latitude NA the main reduction of the negative heat flux feedback below its upper bound ($\alpha_{upper} \approx 35 \text{ W m}^{-2} \text{ K}^{-1}$ here) is provided, not by the WES feedback ($d\alpha_{dyn}$ never $< -10 \text{ W m}^{-2} \text{ K}^{-1}$, Fig. 6c), but by thermodynamic adjustment of the atmosphere ($d\alpha_{thdyn}$ consistently $< -20 \text{ W m}^{-2} \text{ K}^{-1}$ in this region, Fig. 6a).

5 Conclusion and discussion

The main results of this study can be summarized as follows:

- The spatial structure of the magnitude of the SST air-sea heat flux feedback, as estimated in the literature, can be understood from the climatological background state of the MABL and its thermodynamic adjustment to SST anomalies.
- Weak heat flux feedbacks ($\approx 5\text{--}10 \text{ W m}^{-2} \text{ K}^{-1}$) found in the subpolar gyre of the NA and near the margin of the Antarctic winter-time sea-ice edge reflect a regime where there is a large adjustment of the MABL to SST anomalies. This result also applies to SST anomalies of basin-wide spatial scales in the NA and the SO.
- The Gulf Stream and southwestern NA subtropical gyre are highlighted as the region displaying the largest heat flux feedback ($\approx 40 \text{ W m}^{-2} \text{ K}^{-1}$). These reflect a compensation between a moderate thermodynamic adjustment of the MABL to SST anomalies, which tends to weaken the heat flux feedback, and a strengthening of the surface winds, which tends to enhance it.
- The fact that the thermodynamic adjustment of the MABL increases towards large spatial scales is expected from the weakening of lateral advection with spatial scale. It is however more surprising to find that the MABL in high latitudes also shows a large degree of thermodynamic adjustment on shorter (synoptic) scales. Here it is hypothesized that this results from the convergence of moist static energy by synoptic motions and stationary waves over these regions in the annual mean, limiting the ability of the MABL to laterally or vertically export heat or moisture anomalies. Further work is required to fully test this hypothesis.

Overall, the fact that the spatial structure of the heat flux feedback, including high Southern latitudes, can be understood from the “fast” and “slow export” limits, discussed in Sect. 2, provides confidence in the available estimates of feedbacks from data. It is in particular reassuring that oceanic regions near the winter-time sea-ice edge in the SO behave similarly to those in the NA subpolar gyre where confidence in the reanalysis is greater. Note that the analysis presented in this paper has been repeated with the OAF flux dataset (Yu et al. 2008) and the major conclusions, as listed above, are found to be robust. This suggests that available data-based estimates can provide guidance in the interpretation of coupled model integrations with discrepant inherent air-sea restoring time scales (e.g. Ferreira et al. 2015).

Finally, it is worth emphasizing the weak heat flux feedbacks found at high latitudes. For a mixed-layer depth of 100 m, a $10 \text{ W m}^{-2} \text{ K}^{-1}$ feedback strength would, in the absence of other damping processes, lead to a persistence time of SST anomalies of more than a year (≈ 15 months). This suggests that the surface thermal restoring typically used in ocean-only models may be much stronger than data indicate at high latitudes.

Acknowledgments Ute Hausmann and John Marshall acknowledge support by the FESD program of NSF.

Appendix 1: Estimating the heat flux feedback

The heat flux feedback α as defined in (2) is estimated from timeseries of turbulent heat fluxes Q and SST T using lagged covariance analysis, as introduced by Frankignoul et al. (1998). Here we follow the method for seasonal feedback estimation described by Hausmann et al. (2016, i.e. as used to construct their Fig. 6). As therein major sources of low frequency variability (linear seasonal ENSO signals and trends) are removed from anomaly time series before the analysis. The feedback is then obtained for each month of the year as the $T' Q'$ covariance function, weighted by the T' autocovariance

$$\alpha = \frac{\overline{T'(t)Q'(t + 1\delta t)}}{\overline{T'(t)T'(t + 1\delta t)}}, \quad (12)$$

in which δt is one month and t is taken only in certain months of the year. For example, the February (F) feedback $\alpha(F)$ is obtained taking t only in January and February (JF), that is from the response of February and March (FM) heat fluxes to JF SST, weighted by the latter’s own decay into FM: $\alpha(F) = \frac{\overline{T'(JF)Q'(FM)}}{\overline{T'(JF)T'(FM)}}$. The annual-mean feedback displayed in Fig. 2 is then obtained as the average of the feedbacks estimated separately for each month of the year.

Appendix 2: Decomposition of the heat flux feedback into thermodynamic and dynamic components

The turbulent heat flux feedback can be written as $\alpha = \alpha_{upper} + d\alpha$, and $d\alpha$ (mapped in Fig. 3) is further decomposed as (11). Therein the thermodynamic component, $d\alpha_{thdyn}$, reflects the contribution to the feedback, in departure from its upper bound, by thermal and moisture adjustments to SST anomalies (with the other properties of the MABL held fixed). It is given by the sum of the 2nd terms on the rhs of Eqs. (3) and (4), i.e.

$$d\alpha_{thdyn} = -\left(\overline{\rho^a u^a c_{Sp}^a} \partial \langle T^{a'} \rangle / \partial T' + \overline{\rho^a u^a c_{L\bar{L}}} \partial \langle q^{a'} \rangle / \partial T'\right). \quad (13)$$

To estimate (13) from data, $\partial \langle T^{a'} \rangle / \partial T'$ and $\partial \langle q^{a'} \rangle / \partial T'$ are obtained for each month of the year by applying the same lagged covariance analysis method as used for α (see Appendix 1), which gives $\partial \langle X' \rangle / \partial T'$ with $X = Q$, to $X = T^a$ and q^a . The other variables in (13) are estimated from monthly air-sea climatology, as in the estimate of the bounds in Sect. 3a. To capture seasonal correlations, the products in (13) are evaluated for each month of the year, before annually averaging. The result is mapped in Fig. 6a, b.

At the level of approximation used in Sect. 2,

$$d\alpha_{thdyn} \approx d\alpha_{therm} + d\alpha_{rhum}, \quad (14)$$

in which the thermal adjustment contribution ($d\alpha_{therm}$, mapped in Fig. 5c, d) is given by the sum of the 2nd terms on the rhs of (3) and (8) as:

$$d\alpha_{therm} = \overline{\rho^a u^a} \left(\overline{c_{Sp}^a} + \overline{c_{L\bar{L}RH}} \frac{dq_{sat}}{dT} \Big|_{\bar{T}^a} \right) \partial \langle T^{a'} \rangle / \partial T', \quad (15)$$

and the relative humidity adjustment contribution is given by the 3rd term on the rhs of (8) as:

$$d\alpha_{rhum} = -\overline{\rho^a u^a c_{L\bar{L}RH}} \partial \langle r_H' \rangle / \partial T'. \quad (16)$$

Estimation of these terms reveals that the residual of the approximation (14) lies within $\pm 0.5 \text{ W m}^{-2} \text{ K}^{-1}$ everywhere in NA and SO (not shown). Differences between $d\alpha_{thdyn}$ (Fig. 6a, b) and $d\alpha_{therm}$ (Fig. 5c, d) are thus accounted for by the relative humidity adjustment contribution $d\alpha_{rhum}$ (not shown).

The dynamical coupling contribution to the feedback, solely reflecting wind speed adjustments to SST anomalies $\partial \langle u^{a'} \rangle / \partial T'$, is obtained by evaluating (2) while keeping all MABL properties but u^a fixed, and then subtracting α_{upper} , with the result:

$$d\alpha_{dyn} = \left(\overline{\rho^a c_{Sp}^a} (\bar{T} - \bar{T}^a) + \overline{\rho^a c_{L\bar{L}}} (q_{sat}(\bar{T}) - \bar{q}^a) \right) \partial \langle u^{a'} \rangle / \partial T'. \quad (17)$$

The remaining contribution $d\alpha_{res}$ is then estimated as residual of the terms quantified in Eq. (11), that is as:

$$d\alpha_{res} = \alpha - (\alpha_{upper} + d\alpha_{thdyn} + d\alpha_{dyn}). \quad (18)$$

References

Chelton DB, Schlax MG, Freilich MH, Milliff RF (2004) Satellite measurements reveal persistent small-scale features in ocean winds. *Science* 303(5660):978–983

- Czaja A, Marshall J (2001) Observations of atmosphere-ocean coupling in the North Atlantic. *Q J R Meteorol Soc* 127:1893–1916
- Czaja A, van der Vaart P, Marshall J (2002) A diagnostic study of the role of remote forcing in tropical Atlantic variability. *J Clim* 15:3280–3290
- Dee DP, Uppala SM, Simmons AJ, Berrisford P, Poli P, Kobayashi S, Andrae U, Balmaseda MA, Balsamo G, Bauer P, Bechtold P, Beljaars ACM, van de Berg L, Bidlot J, Bormann N, Delsol C, Dragani R, Fuentes M, Geer AJ, Haimberger L, Healy SB, Hersbach H, Hlm EV, Isaksen L, Kllberg P, Khler M, Matricardi M, McNally AP, Monge-Sanz BM, Morcrette JJ, Park BK, Peubey C, de Rosnay P, Tavolato C, Thpaut JN, Vitart F (2011) The ERA-Interim reanalysis: configuration and performance of the data assimilation system. *Q J R Meteorol Soc* 137(656):553–597. doi:10.1002/qj.828
- Fairall CW, Bradley EF, Hare JE, Grachev AA, Edson JB (2003) Bulk parameterization of air-sea fluxes: updates and verification for the COARE algorithm. *J Clim* 16(4):571–591
- Ferreira D, Frankignoul C, Marshall J (2001) Coupled ocean-atmosphere dynamics in a simple midlatitude climate model. *J Clim* 14:3704–3723
- Ferreira D, Marshall J, Bitz CM, Solomon S, Plumb A (2015) Antarctic ocean and sea ice response to ozone depletion: a two timescale problem. *J Clim* 28:1206–1226. doi:10.1175/JCLI-D-14-00313.1
- Frankignoul C (1985) Sea surface temperature anomalies, planetary waves and air-sea feedback in the middle latitudes. *Rev Geophys* 23:357–390
- Frankignoul C, Kestenare E (2002) The surface heat flux feedback. Part I: estimates from observations in the Atlantic and the North Pacific. *Clim Dyn* 19:633–647
- Frankignoul C, Czaja A, L'Heveder B (1998) Air-sea feedback in the North Atlantic and surface boundary conditions for ocean models. *J Clim* 11:2310–2324
- Gill AE (1982) *Atmosphere-Ocean dynamics*. International geophysics series, vol 30. Academic Press, London
- Haney RL (1971) Surface thermal boundary condition for ocean circulation models. *J Phys Oceanogr* 1:241–248
- Hausmann U, Czaja A, Marshall J (2016) Estimates of air-sea feedbacks on sea surface temperature anomalies in the Southern Ocean. *J Clim* 29:439–454. doi:10.1175/JCLI-D-15-0015.1
- Liu WT, Tang W, Niiler PP (1991) Humidity profiles over the ocean. *J Clim* 4(10):1023–1034
- O'Neill LW, Chelton DB, Esbensen SK (2012) Covariability of surface wind and stress responses to sea-surface temperature fronts. *J Clim* 25:5916–5942
- Park S, Deser C, Alexander MA (2005) Estimation of the surface heat flux response to sea surface temperature anomalies over the global oceans. *J Clim* 18:4582–4599
- Rahmstorf S, Willebrand J (1995) The role of temperature feedback in stabilizing the thermohaline circulation. *J Phys Oceanogr* 25:787–805
- Trenberth KE, Caron JM, Stepaniak DP (2001) The atmospheric energy budget and implications for surface fluxes and ocean heat transport. *Clim Dyn* 17:259–276
- Yu L, Jin X, Weller RA (2008) Multidecade global flux datasets from the Objectively Analyzed Air-sea Fluxes (OAFlux) project: latent and sensible heat fluxes, ocean evaporation, and related surface meteorological variables. Woods Hole Oceanographic Institution, OAFlux Project Technical Report OA-2008-01